

Article

Cation exchange induced transformation of InP magic-sized clusters

Jennifer L. Stein, Molly Steimle, Maxwell W. Terban, Alessio Petrone, Simon J. L. Billinge, Xiaosong Li, and Brandi M. Cossairt

Chem. Mater., **Just Accepted Manuscript** • DOI: 10.1021/acs.chemmater.7b03075 • Publication Date (Web): 18 Aug 2017

Downloaded from <http://pubs.acs.org> on August 19, 2017

Just Accepted

“Just Accepted” manuscripts have been peer-reviewed and accepted for publication. They are posted online prior to technical editing, formatting for publication and author proofing. The American Chemical Society provides “Just Accepted” as a free service to the research community to expedite the dissemination of scientific material as soon as possible after acceptance. “Just Accepted” manuscripts appear in full in PDF format accompanied by an HTML abstract. “Just Accepted” manuscripts have been fully peer reviewed, but should not be considered the official version of record. They are accessible to all readers and citable by the Digital Object Identifier (DOI®). “Just Accepted” is an optional service offered to authors. Therefore, the “Just Accepted” Web site may not include all articles that will be published in the journal. After a manuscript is technically edited and formatted, it will be removed from the “Just Accepted” Web site and published as an ASAP article. Note that technical editing may introduce minor changes to the manuscript text and/or graphics which could affect content, and all legal disclaimers and ethical guidelines that apply to the journal pertain. ACS cannot be held responsible for errors or consequences arising from the use of information contained in these “Just Accepted” manuscripts.

Cation exchange induced transformation of InP magic-sized clusters

Jennifer L. Stein, † Molly I. Steimle, † Maxwell W. Terban, ‡ Alessio Petrone, † Simon J. L. Billinge, ‡# Xiaosong Li, † Brandi M. Cossairt*†

†Department of Chemistry, University of Washington, Seattle, Washington 98195-1700, United States

‡Department of Applied Physics and Applied Mathematics, Columbia University, New York, New York 10027, United States

Condensed Matter Physics and Materials Science Department, Brookhaven National Laboratory, Upton, NY 11973, United States

ABSTRACT: Magic-sized clusters (MSCs) can provide valuable insight into the atomically precise progression of semiconductor nanocrystal transformations. We report the conversion of an InP MSC to a Cd₃P₂ MSC through a cation exchange mechanism and attempt to shed light on the evolution of the physical and electronic structure of the clusters during the transformation. Utilizing a combination of spectroscopic (NMR/UV-Vis) and structural characterization (ICP-OES/MS/PXRD/XPS/PDF) tools, we demonstrate retention of the original InP MSC crystal lattice as Z-type ligand exchange initially occurs. Further cation exchange induces lattice relaxation and a significant structural rearrangement. These observations contrast with reports of cation exchange in InP quantum dots, indicating unique reactivity of the InP MSC.

INTRODUCTION

Cation exchange is a widely-utilized tool for accessing colloidal nanomaterials with unique or emergent properties that may be difficult to directly synthesize using conventional nucleation and growth mechanisms. This facile reaction employs the anionic sublattice as a template while cations partially or fully exchange, typically retaining the original crystallite size and shape. Experimental conditions have been developed to access a wide variety of doped nanocrystals,¹⁻⁴ anisotropic structures,⁵⁻⁸ alloyed nanocrystals,^{4,9,10} nanocrystalline heterostructures,¹⁰⁻¹³ and semiconductor nanocrystals that are synthetically challenging to produce *via* a direct route.¹⁴ Chemists have continued to develop this technique by extracting general design principles through examination of ion exchange thermodynamics and consideration of the shared similarities with solid-state ion exchange occurring over a reaction zone, and by probing mechanism using a combination of theory, dynamic simulations, and experiment.¹⁵⁻²³

Magic-sized clusters (MSCs) represent the interface between small molecules and quantum-confined nanostructures. MSCs are atomically-precise clusters with elevated thermodynamic stability compared to structures of similar size that can play a role in nanocrystal nucleation and growth.²⁴ MSCs may serve as a unique tool for studying both the mechanism and structural consequences of cation exchange in nanoscale materials because of their perfect monodispersity and the homogeneity of their surface chemistry. Utilizing clusters as models to provide insight into the nature of cation exchange in nanocrystals has most recently been demonstrated by the Jain group in their examination of the progression of CdSe MSCs to Cu₂Se clusters.²⁵ Due to the presence of a metastable cluster intermediate, they demonstrated that the Cd²⁺ sublattice experienced reorganization to a six-coordinate structure upon initial introduction of Cu⁺ dopant ions. The six-coordinate structure had a greater affinity for further Cu⁺ dopants, supporting the co-operative nature of cation exchange observed in the analogous nanocrystal-scale reaction.^{25,26} This work adds to the growing body of information on cation exchange in metal chalcogenide lattices,^{16,18} however much remains to be explored with other lattice types.

Among the few reports of cation exchange in non-chalcogenide lattices,^{11,27-29} Beberwyck and Alivisatos reported the use of Cd₃P₂ and Cd₃As₂ quantum dots as templates to In/Ga pnictides through cation exchange and highlighted the significant differences that exist between ion exchange reactions in nanocrystal lattices with different levels of ionic and covalent character.¹⁴ While many II-VI ion exchange reactions can be performed reversibly at room temperature, the III-V reactions shown in their work were irreversible and required sequential exchanges at higher temperatures to drive the reaction to completion, with Cd²⁺ cations remaining in the final material even under optimized conditions. Interested in learning more about cation exchange in phosphide lattices, we sought to extend the MSC approach to this system.

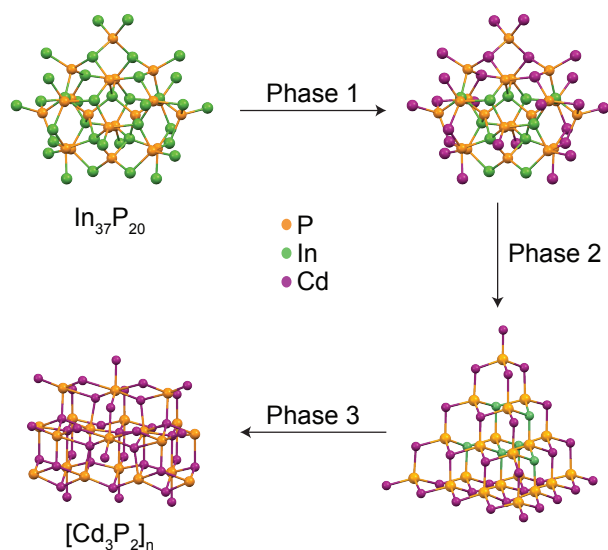
Recently, a diffraction quality single crystal of In₃₇P₂₀(O₂CCH₂Ph)₅₁, an InP MSC, was isolated and structurally characterized to reveal a strained [In₂₁P₂₀]³⁺ inorganic core ligated by 16 additional indium atoms and an interconnected network of 51 bidentate and mostly bridging carboxylate ligands.³⁰ Our lab has observed that the InP MSC displays site selective reactivity when exposed to moist air, leading to a carboxylate ligand shift (bidentate to monodentate) in order to accommodate a water molecule bound to an indium. To explore this site-selective modification further, we examined the reactivity of the InP MSC in the presence of other Lewis bases; exposure to primary amines indicated that these ligands initiate indium carboxylate desorption and ultimately lead to structural rearrangement of the cluster.³¹ Thus, utilizing InP MSCs as templates for cation exchange reactions towards new cluster materials with the ability to predict the progression of the reaction was of great interest to us.

RESULTS AND DISCUSSION

Herein we report the transformation of InP MSCs to Cd₃P₂ MSCs at room temperature where full conversion to Cd₃P₂ can be achieved at a 500:1 excess of cadmium carboxylate per InP cluster. The final product is physically and electronically indistinguishable from the Cd₃P₂ MSC prepared independently from molecular precursors (Figure S1).³² The Cd₃P₂ MSC is characterized by narrow absorption and emission features at 450 and 455 nm, respectively, and weak

band-edge photoluminescence (<3% quantum yield). Although the crystal structure of Cd_3P_2 MSCs is unknown, it is characteristically different from the bulk tetragonal crystal.^{32,33} To probe potential intermediates during this cation exchange process, the reaction between $\text{In}_{37}\text{P}_{20}(\text{O}_2\text{CCH}_2\text{Ph})_{51}$, ($\text{O}_2\text{CCH}_2\text{Ph} = \text{PA}$), with stoichiometric amounts of cadmium carboxylate was monitored. Using a combination of optical and nuclear magnetic resonance (NMR) spectroscopy together with a variety of structural and analytical characterization tools, we outline the step-wise mechanism by which InP MSCs undergo cation exchange with Cd^{2+} (Scheme 1).

Scheme 1. Proposed mechanism of the conversion of InP MSCs to Cd_3P_2 MSC via cation exchange. Three distinct phases are proposed: phase 1 is a topotactic process that is dominated by Z-type ligand exchange, phase 2 involves a relaxation of the strained cluster lattice on further incorporation of cadmium, and phase 3 is the final structural transformation that accompanies complete exchange of cadmium for indium in the lattice. The Cd_3P_2 MSC has an unknown crystal structure, thus the authors have chosen to visually represent the final structure as a tetragonal portion derived from the bulk Cd_3P_2 lattice (pdf #01-070-3099 ICSD).



We propose that cation exchange is initiated through Z-type ligand exchange between indium and cadmium carboxylates. Z-type ligands (Lewis acids or two-electron acceptors) have been shown to reversibly bind and exchange with anionic sites on nanocrystal surfaces with no impact on crystal structure or strain, although both examples are isovalent cases in which ligand density remains unchanged.^{34,35} This initial topotactic phase (phase 1) conserves the structure of the $\text{In}_{21}\text{P}_{20}$ charged core while the metal carboxylates on the surface undergo exchange. We then observe relaxation of the crystal lattice to a structure consistent with a zinc blende assignment, which we designate as phase 2. Through the addition of excess Cd^{2+} , we hypothesize that increasing amounts of cadmium replacing indium in the core induces structural relaxation of the initially strained pseudo-tetrahedral coordination environments. Finally, phase 3 is characterized by the distinct transition to Cd_3P_2 which can occur abruptly with no indication of an intermediate product.

Phase 1: Topotactic cation exchange

The evolution of the absorption spectra as cadmium phenylacetate ($\text{Cd}(\text{PA})_2$) was progressively added to a solution of

$\text{In}_{37}\text{P}_{20}(\text{PA})_{51}$ is shown in Figure 1. Each spectrum in this titration represents the thermodynamic endpoint of the reaction between the two reagents at a given cadmium concentration at room temperature. Although absorbance measurements do not provide insight on the precise structural changes occurring, they are a diagnostic fingerprint of the cluster evolution. During phase 1, the InP MSC peak at 386 nm is broadened with a more pronounced shoulder at 430 nm that is present up to 37 equivalents of $\text{Cd}(\text{PA})_2$. ^{31}P NMR has proven to be a useful tool to examine structural evolution of the cluster because the unique phosphorus environments in the *pseudo-C₂-symmetric* $\text{In}_{37}\text{P}_{20}(\text{O}_2\text{CCH}_2\text{Ph})_{51}$ cluster have allowed peak assignment based on chemical shielding arguments and integration, and may be telling of specific site reactivity with cadmium.³¹ With one equivalent of cadmium, the original anionic sublattice appears to be maintained with slight changes in the chemical shielding tensors as is expected upon a change in surface ligation (Figure 2). The addition of up to 5 equivalents lead to a broadening and slight upfield shift of all resonances. In accordance with the characteristic chemical shift of Cd_3P_2 MSCs at -364 ppm, we suggest that the upfield shift is evidence for the formation of cadmium-phosphorus bonds.

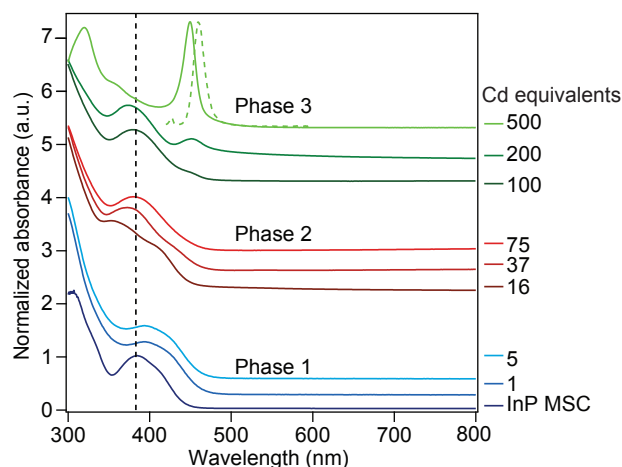


Figure 1. UV-Vis absorbance traces (solid, offset) of InP MSCs exposed to increasing equivalents of $\text{Cd}(\text{PA})_2$ relative to a single InP MSC. Photoluminescence of Cd_3P_2 final product (dashed). The dashed black line is to direct the eye towards the shift from the initial InP MSC peak at 386 nm.

Elemental analysis was necessary to help corroborate the spectroscopic data and more importantly, to confirm that cadmium was coordinating to the cluster. To purify the samples of excess metal carboxylate, multiple rounds of gel permeation chromatography were carried out with the purification endpoint confirmed by unchanging molar ratios upon analysis by inductively coupled plasma optical emission spectrometry (ICP-OES). The molar ratios extracted from ICP-OES analysis are shown in Table 1 and have all been normalized to 20 P to allow comparison with the composition of the initial $\text{In}_{37}\text{P}_{20}$ cluster. These data support the hypothesis that the core $[\text{In}_{21}\text{P}_{20}]^{3+}$ composition is maintained up to the addition of 16 equivalents of $\text{Cd}(\text{PA})_2$ with the surface indium atoms being progressively replaced by cadmium.

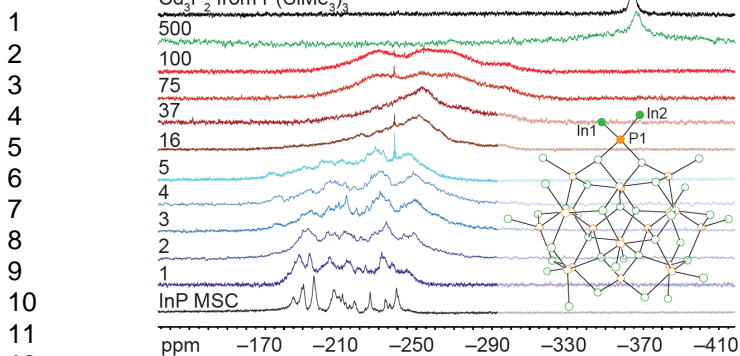


Figure 2. ^{31}P NMR (283.5 MHz, C_6D_6) spectra of clusters and increasing cadmium equivalents taken at room temperature. Trace colors correspond to the assignment of phase 1, 2, or 3. The sharp peak at -240 ppm is a PH_3 impurity ($< 0.1\%$ of total P). Inset of $\text{In}_{37}\text{P}_{20}(\text{PA})_{51}$ crystal highlighting apical indium atoms with ligands removed for clarity.

Table 1. Molar ratios of InP, intermediate, and Cd_3P_2 cluster species by ICP-OES. Compositional analysis by x-ray photoelectron spectroscopy was performed on several samples to verify ICP-OES measurements (Table S1).

Sample	Cd	In	P
$\text{In}_{37}\text{P}_{20}$	0	40	20
1	1.8	46	20
5	12	34	20
16	28	28	20
37	55	36	20
75	82	33	20
100	68	28	20
200	69	5	20
Cd_3P_2 via $\text{P}(\text{SiMe}_3)_3$	60	0	20

Additionally, matrix-assisted laser desorption/ionization coupled with time-of-flight mass spectrometry (MALDI-TOF) was performed on the InP MSC and on the Cd-treated intermediates (Figure S2). Due to the unknown nature of how the clusters fragment, the broad distributions of fragment masses were analyzed with Gaussian fits to extract characteristic trends (Table S2). The InP MSC shows a parent fragment ion centered at 8570 m/z, similar to what has been observed for InP clusters formed during InP QD synthesis,³⁶ with the narrowest Gaussian distribution (FWHM = 980). The mass of an intact fully ligated cluster is $11,759$ g/mol so we expect that a portion of the cluster surface is lost during ionization. While the mass distribution consistently broadens as the cation exchange progresses, the addition of ≤ 16 equivalents of Cd^{2+} results in no significant change in the parent fragment ion mass. Consistent with the ICP-OES interpretation, this suggests the parent fragment

ion is unaffected by initial surface cation exchange. While the former data certainly suggest that the original cluster crystal remained intact, more precise structural characterization was necessary to ascertain whether this process was topotactic in nature.

Comparing the physical structures of cadmium-coated or cadmium-alloyed intermediates is possible through powder X-ray diffraction (PXRD) and atomic pair distribution function (PDF) analysis. PDF has previously been used to reveal that InP MSCs with different ligand sets (phosphonate terminated vs carboxylate terminated) have very different internal structures.³⁷ PDF analysis of $\text{In}_{37}\text{P}_{20}$ and the resulting Cd-treated products demonstrates that the core structure is maintained up to the addition of 16 equivalents of $\text{Cd}(\text{PA})_2$ (Figure 3A, Figure S3). Furthermore, we used the predicted structure of $\text{Cd}_{16}\text{In}_{21}\text{P}_{20}$, in which the 16 surface indium were exchanged with cadmium, to simulate the PDF. This computed pattern correctly predicts many of the minor changes experimentally measured by the cluster reacted with 16 equivalents of cadmium (Figure S4). Direct analysis of the PXRD data demonstrates that no shifts are present that would correspond to additional lattice strain/relaxation or alloying. In fact, the powder diffraction pattern of InP MSCs already differs from larger QDs and bulk InP due to the low-symmetry and strain present in the core thus PXRD can be very telling of changes in the InP cluster lattice.³⁰

The data thus far suggests that cation exchange occurs in a topotactic fashion, conserving the structure of the inorganic core. We expect that the exchange initially takes place at the most reactive indium sites, especially because these reactions are performed at room temperature. More specifically, based on our prior work with the addition of Lewis bases to InP MSCs,³¹ we envision cation exchange beginning with Z-type ligand exchange to replace the apical indium atoms (In1/2 in Figure 2).

Computational analysis of an InP cluster with cadmium replacing the apical indium (In1/In2) resulted in a slight red-shifted absorbance shoulder, consistent with our experimental observations (Figure S5). In comparison, the model where equatorial indium atoms were exchanged by cadmium leads to a calculated absorbance spectrum with a significantly red-shifted lowest energy electronic transition (Figure S5). In this last model, the Cd^{2+} atoms are now situated in the physical region where most of the electronic density of the HOMO is spatially localized (Figure S6) and therefore the two electronic transitions responsible for the first peak absorption (HOMO-1 to LUMO and HOMO to LUMO) are strongly impacted. These data are indicative that cation exchange likely begins by Z-type ligand exchange at these apical sites while the structure of the phosphide sublattice is largely unperturbed. Without a diffraction quality single crystal, it is difficult to identify whether some cadmium has intercalated into the $[\text{In}_{21}\text{P}_{20}]^{3+}$ core before stoichiometric exchange on the surface has completed but we hypothesize that it would be a minor amount before the next phase of the cation exchange process occurs, which involves a structural rearrangement (phase 2).

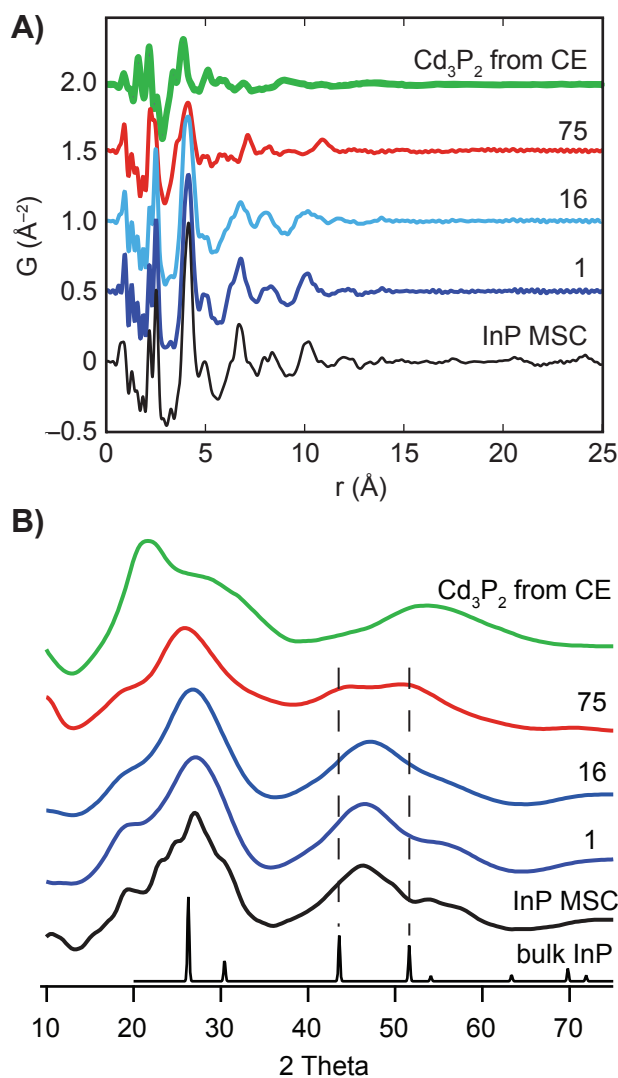


Figure 3. (A) Measured PDFs for the series of InP MSCs with increasing equivalents of cadmium added starting with pure InP. (B) powder X-ray diffraction patterns of corresponding PDF samples with bulk InP (pdf #01-073-1983 ICSD).

Phase 2: Structural relaxation

We categorize phase 2 as a distinct event due to the structural changes observed by PDF and XRD. By 75 equivalents of Cd^{2+} , alteration of the scattered intensities and drastic changes in the PDF signal indicate structural reconstruction, suggesting the exchange of cadmium into the core (Figure 3). Furthermore, this PDF matches well with a zinc blende tetrahedron containing 35 Cd and 20 P atoms, similar to that seen for CdSe MSCs (Figure S7).³⁸ PXRD analysis suggests that the lattice has relaxed to a zinc blende structure (represented by the bulk InP powder diffraction pattern) with major reflections at 26, 43.6 and 51.6 2θ , correlating with the PDF fits.

Absorbance measurements show that above 37 equivalents of cadmium, the excitonic feature blue-shifts to an intermediate that is reproducibly observed between 360-370 nm depending on the specific identity of the ligand (Figure 1). By ^{31}P NMR spectroscopy, this phase is not characterized by precisely defined phosphorus chemical environments, rather we observe a continuous upfield shift and broadening of all resonances as the cadmium content in the phosphide sublattice continues to increase (Figure 2). This may indicate

that cadmium exchange into the core is non-selective, giving rise to a range of structures in which varying specific indium atoms have been replaced by cadmium. Quantitative ^{31}P NMR spectroscopy indicates that the amount of phosphorus contained in these cluster species is conserved through the course of the cation exchange, supporting an anionic rearrangement step without anion loss (Figure S8). The presence of additional cadmium is verified by compositional analysis in which the molar ratios show an increasing amount of cadmium. Further interpretation of the ICP data is somewhat unclear (likely due to the presence of a large excess of cation loosely interacting with the cluster surface),^{39,40} but suggests that significant concentrations of indium remain in the sample with super-stoichiometric addition of $\text{Cd}(\text{PA})_2$. Mass spectrometry supports the incorporation of additional cadmium at higher concentrations in which a domain of larger masses is observed, relative to the phase 1 mass distributions (Figure S2, Table S1). The mass of the parent fragment ion rises by approximately 1 kDa and remains nearly invariable thereafter, consistent with a structural change initiated above 16 equivalents of Cd^{2+} that impacts the cluster fragmentation.

Although we attribute the progression of cluster species in phase 2 as a continuation of cation exchange between core indium and cadmium that results in structural reorganization to a relaxed zinc blende species, the pathway by which this occurs is still unknown. Accounting for the difference in charge additionally introduces complications in assigning a diffusion pathway, beyond surface-related exchanges, through interstitial sites or by a vacancy-assisted mechanism.^{7,15,23} The extent of a detailed mechanistic examination is beyond the scope of this current study but certainly of interest to the authors.

Phase 3: Reconstruction to Cd_3P_2

At high equivalents of $\text{Cd}(\text{PA})_2$ (100, 200, and 500 equivalents), a new absorbance feature at 450 nm appears in the UV-Vis spectrum (Figure 1), which is characteristic of a known Cd_3P_2 MSC.³² The InP cluster has negligible room temperature photoluminescence (PL) but once conversion to Cd_3P_2 is complete, weak band-edge PL (<1% quantum yield) is measured. In order to compare the Cd_3P_2 produced *via* cation exchange (CE), Cd_3P_2 clusters were independently synthesized following the literature procedure described by Yu and co-workers with slight modifications.³² Briefly, cadmium carboxylate was dissolved in toluene and $\text{P}(\text{SiMe}_3)_3$ was injected at room temperature. The reaction proceeded at room temperature but could be carried out up to 120 °C.

Monitoring the *in-situ* growth of Cd_3P_2 following $\text{P}(\text{SiMe}_3)_3$ injection supports a homogeneous growth mechanism with a continuous increase in cluster size towards the thermodynamically stable product with an absorption maximum at 450 nm (Figure S9a). Slight shifts in the absorption maxima occur depending on the precise identity of the supporting ligands (oleate or phenylacetate). Monitoring the *in-situ* synthesis of Cd_3P_2 *via* introduction of 500 equivalents Cd^{2+} to InP MSCs also shows a continuous transition from the InP MSCs to the Cd_3P_2 MSCs with no observable intermediates (Figure S9b) and demonstrates that InP MSCs do not re-dissolve to form new Cd-P monomers. This continuous growth appeared to conflict with the evolution of absorbance features at <100 equivalents Cd^{2+} , but we hypothesize that a supersaturated solution of Cd^{2+} with InP MSCs likely precludes the buildup of any kinetic products and that rapid exchange and rearrangement occurs without cluster dissolution. Notably, if the stable phase 2 intermediate with diagnostic UV-Vis absorption at 360/370 nm formed by addition of 75

equivalents Cd^{2+} is treated with additional Cd^{2+} , a continuous progression towards Cd_3P_2 is observed, demonstrating that the intermediates are viable precursors on the pathway towards Cd_3P_2 (Figure S10). The alternative possibility that clusters re-dissolve in the presence of excess cadmium to form a short-lived monomer species was strongly considered, but the lack of spectroscopic evidence, especially from *in-situ* absorbance measurements, lead us to the conclusion that the crystal lattice is conserved during rearrangement.

Structurally, the two products are comparable by ^{31}P NMR spectroscopy. Cd_3P_2 clusters synthesized by $\text{P}(\text{SiMe}_3)_3$ injection show a single peak in the ^{31}P NMR spectrum at -364 ppm, consistent with literature reports,³² which indicates that the Cd_3P_2 cluster has a very symmetric structure with contributions to the broad linewidth likely arising from differences in surface and core Cd-P environments. The final Cd_3P_2 product produced by cation exchange has a single peak at -366 ppm demonstrating that there are likely no residual In-P bonds remaining. As expected, following purification, the composition of *in-situ* synthesized and cation exchange produced Cd_3P_2 are nearly identical with the presence of a negligible amount of indium in the cation exchange sample (Table 1).

Since the bulk and cluster phosphorus NMR differ greatly, it is no surprise that by PXRD the measured pattern does not overlay well with the reported bulk Cd_3P_2 patterns (Figure S11).^{32,33} This is consistent with previous characterization of the Cd_3P_2 cluster, which shows a similarly broad powder pattern.^{32,41} Previous measurements of Zn_3P_2 nanocrystal powder diffraction patterns, which shares the tetragonal lattice, have shown a divergence from the bulk structure at small nanocrystal sizes, consistent with the complexity of the 40-atom tetragonal unit cell.^{42,43} Furthermore, PDF analysis indicates that the final product of cation exchange is demonstrably different from the other measured samples, indicating a final structural transformation has occurred on complete conversion to Cd_3P_2 (Figure 3, S12). Although the use of transmission electron microscopy (TEM) would help reveal changes in particle morphology throughout this transformation, the poor contrast of InP and sub-2 nm particles limits the application of this technique.^{37,44}

Unique reactivity of InP MSC

In many examples of cation exchange reactions, hard-soft acid-base theory is used to design experimental conditions that will favor the extraction of the Lewis acid from the solid to solution in cases where the formation energy of the desired product is favored.^{15,18} This technique was utilized by Beberwyck and Alivisatos to irreversibly produce InP QDs from Cd_3P_2 QDs at high temperatures in tandem with the addition of soft Lewis bases.¹⁴ In our work, the formation of Cd_3P_2 occurs at room temperature from InP MSCs, which we propose is driven by the formation of the more stable Cd_3P_2 cluster. Under harsher synthetic conditions, the structural integrity of the cluster anionic sublattice is completely disrupted. Analogous to the room temperature reactions, varying concentrations of cadmium heated to 100°C with InP MSCs produce what are likely alloyed nanoparticles due to the decrease of the bandgap with increasing amounts of cadmium (Figure S13). The distinction between InP MSC and QDs is that the inherent strain present in the InP MSC lattice likely lends itself to significantly different reactivity relative to a crystalline QD. Each phase discussed previously involves to some degree a surface reorganization or structural reconstruction that we propose corresponds to an energetic stabilization from the distorted InP MSC lattice.

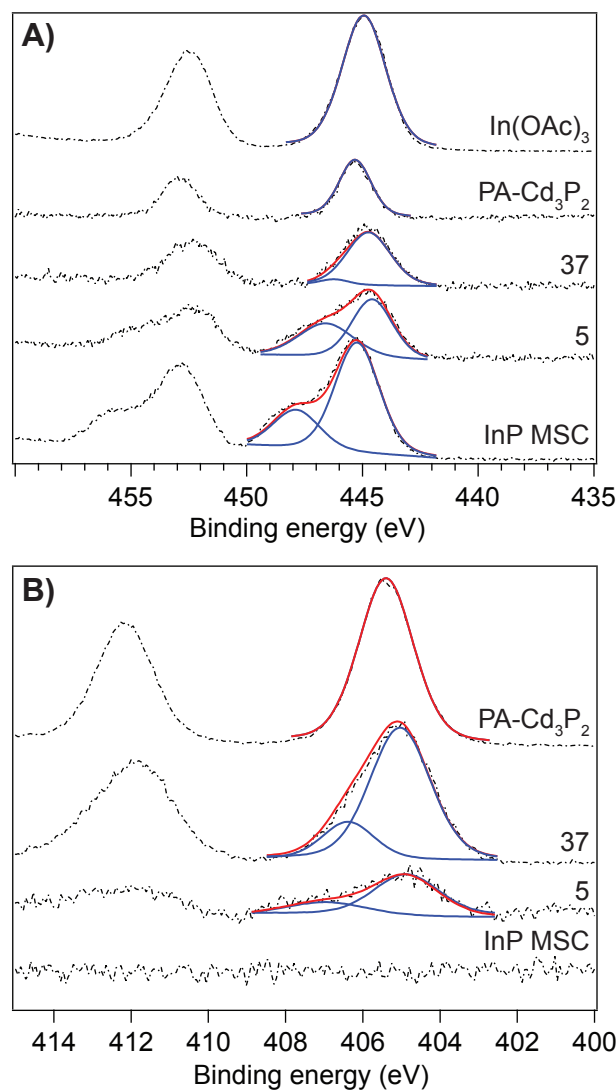


Figure 4. Experimental intensity (black dashed) and fitted profile (red/blue solid) of core level In 3d (a) and Cd 3d (b). Samples are InP MSCs, 5 and 37 equivalents of Cd^{2+} , and PA- Cd_3P_2 is a product of cation exchange with 200 equivalents of $\text{Cd}(\text{PA})_2$. Peak fits and atomic percentages are in Table S2.

Evidence for the presence of significant strain in the InP MSC is provided by analysis of the metrical parameters from the single crystal X-ray diffraction data and is consistent with observed shifts in the measured powder diffraction pattern which show that the lattice is only pseudo-tetrahedral.³⁰ X-ray photoelectron spectroscopy (XPS) demonstrates the differences between nanocrystalline and cluster-sized InP as well. The In 3d region shown in Figure 4a shows a distinct asymmetric peak shape with a main peak at 445.4 eV and a shoulder at 448.0 eV, diverging from the typical Gaussian line shape common to InP QDs.^{45,46} This is mirrored in the second feature resulting from spin-orbit splitting, indicating these features arise from the indium core electrons. As more Cd^{2+} reacts with the cluster, the shoulder shifts to lower binding energies and diminishes. This trend is also observed in the Cd 3d spectra (Figure 4b). Previous reports of core/shell and alloyed structures have described a similar shoulder peak, in which the presence of peak asymmetry corresponds to the presence of a different “surface” component as seen in InP/ ZnS ⁴⁷ and multiple other materials.^{48–50}

We hypothesize that the inherent strain of the $[\text{In}_{21}\text{P}_{20}]^{3+}$ core contributes to diversifying the surface and core components. As structural rearrangement proceeds towards a more symmetric, and presumably less strained Cd_3P_2 structure, the differences between core and surface environments is significantly reduced, leading to coalescence of the signal to one peak in the final Cd_3P_2 MSC. Further evidence supporting the progression towards a more symmetric cluster can be found in the C 1s XPS spectra (Figure S14). It should be noted that while the final phenylacetate-ligated Cd_3P_2 cluster obtained by CE exhibits some signal from indium, compositional analysis of this sample indicates almost negligible concentrations of indium in the sample, which is likely present as loosely associated metal carboxylates.

The reversibility of the cation exchange reaction has been examined as well, further supporting our claim that InP MSCs exist in a higher energy state and re-formation of the original structure is unlikely. Interestingly, addition of In^{3+} to solutions of purified Cd_3P_2 clusters does lead to reaction consistent with indium incorporation, but the observed products are distinct from the intermediates we've characterized here likely due to the nature of the structural evolution described in Scheme 1 (Figures S15/S16).

CONCLUSIONS

From the combined data, we suggest the conversion of InP MSCs into Cd_3P_2 MSCs proceeds according to the mechanism depicted in Scheme 1. Up to 16 surface indium cations are progressively and stoichiometrically replaced by cadmium cations with a requisite lowering in the total ligand density at the cluster surface that is not accompanied by significant structural changes (phase 1). Beyond this point, a large excess of cadmium in solution is required to push progressive exchange with core indium and that this exchange is accompanied by a structural relaxation to the zinc blende structure (phase 2). During titration with Cd^{2+} , we observe that the structural rearrangement to a tetragonal lattice occurs in an abrupt, and potentially irreversible step, with subsequent cation exchange being rapid, leading to the diagnostic optical signatures of the Cd_3P_2 MSC (phase 3). These identifiable steps can be bypassed through the addition of a considerable excess of cadmium to the InP MSCs, which prevents the formation of intermediate kinetic products and progresses directly to Cd_3P_2 .

With respect to previous work on III-V cation exchange in which the reverse reaction of Cd_3P_2 quantum dots to give InP was designated irreversible,¹⁴ we consider the differences in quantum dot and cluster structure to be significant. The strain inherent in the InP MSC lattice likely leads to significant differences in its relative reactivity with Cd^{2+} versus a crystalline zinc blende QD. However, the general principle that stoichiometric Z-type exchange with ligand reorganization precedes thermodynamically-driven cation exchange is likely to be conserved in these systems.

EXPERIMENTAL SECTION

All glassware was dried in a 160 °C oven overnight prior to use. All reactions, unless otherwise noted were run under an inert atmosphere of nitrogen using a glovebox or using standard Schlenk techniques. *Warning: dimethyl cadmium is a volatile and extremely toxic reactant and was handled with care within a nitrogen glovebox. Both dimethyl cadmium and $\text{P}(\text{SiMe}_3)_3$ are pyrophoric, extremely reactive, and should be handled with caution.* Indium acetate (99.99%),

anhydrous oleic acid ($\geq 99\%$), phenylacetic acid (99%), and *trans*-2-[3-(4-*tert*-Butylphenyl)-2-methyl-2-propenyldiene]malononitrile (DCTB) ($\geq 99.0\%$) were purchased from Sigma-Aldrich Chemical Co. and used without further purification. Dimethyl cadmium (97%) was purchased from Strem chemicals and stored in a nitrogen glovebox. Bio-Beads S-X1 were purchased from Bio-Rad Laboratories. Omni Trace nitric acid was purchased from EMD Millipore and used without further purification. 18.2 M Ω was collected from an EMD Millipore water purification system. All solvents, including toluene, pentane, ethyl acetate, and acetonitrile were purchased from Sigma-Aldrich Chemical Co., dried over CaH_2 , distilled, and stored over 4 Å molecular sieves in a nitrogen-filled glove box. C_6D_6 was purchased from Cambridge Isotope Labs and was similarly dried and stored. $\text{P}(\text{SiMe}_3)_3$ was prepared following literature procedures.⁵¹

³¹P NMR spectra were collected on a 700 MHz Bruker Avance spectrometer. UV-Vis spectra were collected on a Cary 5000 spectrophotometer from Agilent or in-situ with an Ocean Optics TI300-Series absorbance dip probe. Data collected from the dip probe were smoothed in Igor Pro with binomial smoothing algorithms. Fluorescence and quantum yield measurements were taken on a Horiba Jobin Yvon FluoroMax-4 fluorescence spectrophotometer with the QuantaPhi integrating sphere accessory. ICP-OES was performed using a Perkin Elmer Optima 8300. TEM images were collected on an FEI Tecnai G2 F20 microscope using an ultrathin carbon film on holey carbon purchased from Ted Pella Inc.

Synthesis of InP MSCs: InP MSCs were synthesized following a modified preparation from Gary *et al.*³⁷ Briefly, indium acetate (934 mg, 3.2 mmol) and phenylacetic acid (1.58 g, 11.6 mmol) were heated at 100 °C overnight under reduced pressure. Dry toluene (10 mL) was added to the reaction flask at room temperature the following day. $\text{P}(\text{SiMe}_3)_3$ (465 μL , 1.6 mmol) was measured into 5 mL of toluene and injected into the indium phenylacetate at 110 °C. Cluster growth was typically complete within 20-40 minutes. Purification of the particles was achieved through successive precipitation/redissolution cycles using toluene and pentane as the solvent and non-solvent, respectively.

Cadmium phenylacetate synthesis: Dimethyl cadmium (559 μL , 7.8 mmol) was added dropwise to a chilled solution of phenylacetic acid (2.12 g, 15.6 mmol) in a 4:1 pentane/toluene mixture. After 3 hours of stirring, volatile solvents were removed under vacuum and the product was washed 3 more times with pentane. The same procedure was used to synthesize cadmium oleate with oleic acid in place of phenylacetic acid and product washes were performed with ethyl acetate instead of pentane.

Cd^{2+} titrations: Stoichiometric amounts of cadmium oleate dissolved in toluene, or cadmium phenylacetate dissolved in acetonitrile, were added to solutions of InP stirring at room temperature. Solutions were monitored by UV-Vis until changes were no longer observed (typically 12-24 hours). The solutions were purified by gel permeation chromatography; preparation of the column in the glovebox was performed following a literature procedure.⁵² Purified samples were characterized by ICP, PDF, XRD, TEM, XPS, and MALDI-TOF.

Cd_3P_2 MSC via molecular precursors: Cadmium phosphide MSCs were synthesized using a modified literature procedure.³² Cadmium oleate (0.135 g, 0.2 mmol) was dissolved in 10 mL dry toluene in a reaction flask under nitrogen. $\text{P}(\text{SiMe}_3)_3$ (15 μL , 0.05 mmol) was measured into 2 mL of toluene and injected into the flask at room temperature. Cluster growth was monitored by UV-Vis until

no further changes occurred. Purification was achieved through successive precipitation/re-dissolution cycles using toluene and ethanol as the solvent and non-solvent, respectively. Particle growth was observed with excess purification, further relevant details are discussed in the SI (Figure S11).

MALDI-TOF: Mass spectra were collected on a Bruker Autoflex II instrument using DCTB as the matrix. Cluster samples dispersed in toluene were mixed with toluene solutions of the matrix and spotted on a stainless steel plate in a glovebox. Desorption and ionization of samples was achieved by irradiation with a pulsed nitrogen laser. Mass spectra were measured with the detector in linear positive mode with a laser intensity between 5-15%. Calibration was performed using external standards ubiquitin I, myoglobin and cytochrome C. Data was smoothed and fitted in Igor Pro using binomial smoothing algorithms.

XPS acquisition: All XPS spectra were taken on a Surface Science Instruments S-Probe photoelectron spectrometer. This instrument has a monochromatized Al K α X-ray source which was operated at 20 mA and 10 kV, and a low energy electron flood gun for charge neutralization. The samples were drop-cast solutions on a Si wafer while the indium acetate was brushed onto two-sided tape mounted on a Si wafer. X-ray analysis area for these acquisitions was approximately 800 μm across. Pressure in the analytical chamber during spectral acquisition was less than 5×10^{-9} torr. All included figures are high resolution spectra. Pass energy for high resolution spectra was 50 eV and data point spacing was 0.065 eV/step. The take-off angle (the angle between the sample normal and the input axis of the energy analyzer) was 0° (~ 100 \AA sampling depth). Service Physics Hawk version 7 data analysis software was used to peak fit high resolution spectra.

Computational methods: Computational studies were performed using the *Gaussian* electronic structure package.⁵³ The HSE06 range-separated hybrid DFT functional was used to perform both the linear-response TDDFT absorption spectra and geometry optimizations.⁵⁴⁻⁵⁶ This method is appropriate for describing charge-transfer excitations and has been previously shown to correctly compute the InP quantum dot electronic structure.^{30,31,57} TDDFT was used to compute both the excitation energies and corresponding oscillator strengths of the first 10 electronic transitions.⁵⁸⁻⁶⁰ The LANL2DZ basis set is used, in which core electrons are replaced by an effective core potential, and only O (1s, 2s, 2p), C (1s, 2s, 2p), In (5s, 5p), Cd (4d, 5s, 5p) and P (3s, 3p) atomic orbitals are described with explicit basis functions.⁶¹⁻⁶⁴

All calculations were performed on structures where the phenyl moieties were replaced by acetate, $\text{In}_{37}\text{P}_{20}(\text{O}_2\text{CCH}_3)_{51}$, $\text{Cd}_2\text{In}_{35}\text{P}_{20}(\text{O}_2\text{CCH}_3)_{49}$, and $\text{Cd}_{16}\text{In}_{21}\text{P}_{20}(\text{O}_2\text{CCH}_3)_{35}(\text{HO}_2\text{CCH}_3)_2$, to investigate the effect of the presence of cadmium atoms on the UV-Vis spectrum, the electronic properties and structural rearrangement. Starting from the optimized $\text{In}_{37}\text{P}_{20}(\text{O}_2\text{CCH}_3)_{51}$ structure, the Cd-containing models were prepared, and further optimized, by replacing two In atoms with two Cd atoms and removing two carboxylate ligands, the closest to the substituted atoms, to preserve the charge compensation, $\text{Cd}_2\text{In}_{35}\text{P}_{20}(\text{O}_2\text{CCH}_3)_{49}$. The substitution strategy mostly retained the overall molecular symmetry, therefore in the resulting models two In atoms, either located on top of the pseudo C_2 symmetry axis (namely axial) of the molecule or in the plane (namely equatorial) orthogonal to it, were substituted by two Cd atoms, respectively. For the 16 Cd-containing structure, starting from the optimized $\text{In}_{37}\text{P}_{20}(\text{O}_2\text{CCH}_3)_{51}$ structure, 14 negative

charged ligands were removed and another two were protonated (located at the opposite sides of the molecule equatorial plane) to preserve both the charge compensation and simultaneously preserve full cadmium coordination and the overall cluster symmetry.

PDF analysis: X-ray total scattering experiments were conducted on beamline 28-ID-2 at the National Synchrotron Light Source II (NSLS-II) at Brookhaven National Laboratory. An X-ray beam of energy 67.563 keV ($\lambda = 0.18351$ \AA) was focused on samples loaded into Kapton capillaries cooled to 100 K using a liquid nitrogen cryostream. Scattered intensities were collected in rapid acquisition mode⁶⁵ on a Perkin-Elmer 2D flat panel detector (2048×2048 pixels and 200×200 μm pixel size) mounted orthogonal to the beam path at a distance of 205.4850 mm from the sample. Final Cd_3P_2 products were measured on a separate date using a similar setup. A Ni standard sample was measured to calibrate the detector geometry, and 2D intensities were azimuthally integrated to 1D intensity versus the magnitude of the scattering vector Q using Fit2D.⁶⁶ Scattering from an empty Kapton tube was measured and subtracted as a background.

The PDF gives the scaled probability of finding atom-pairs in the material at a distance r apart. The program xPDFsuite with PDFGetX3^{66,67} was used to convert the diffracted intensities to the real-space pair distribution function (PDF), $G(r)$, by

$$G(r) = \frac{2}{\pi} \int_{Q_{\min}}^{Q_{\max}} F(Q) \sin(Qr) dQ$$

where $F(Q)$ is the total scattering structure function which is generated after normalization and reduction of the coherent scattering intensities, and Q_{\min} and Q_{\max} are the minimum and maximum values of the scattering momentum transfer considered.

Structure refinements were carried out using the Diffpy-CMI complex modeling framework.⁶⁷ The starting model for InP clusters was obtained from Gary *et al.* from which ligand atoms were removed except for oxygen.³⁰ Model PDFs were generated as in Jensen *et al.*,⁶⁸ by first simulating the structure function from the Debye scattering equation,

$$F(Q) = \frac{1}{N(f(Q))^2} \sum_{i,j \neq i} f_i(Q) f_j(Q) \frac{\sin(Qr_{ij})}{r_{ij}}$$

which was then Fourier transformed over a range of 0.85-23.1 \AA^{-1} , and subsequently refined using isotropic thermal parameters U_{iso} for each atomic species, a scale factor, an expansion coefficient, an r -dependent peak sharpening coefficient δ_2 to account for correlated motion.

ASSOCIATED CONTENT

Supporting Information

Additional details regarding synthetic conditions, computations, and spectra/fits for MALDI-TOF, PDF, and XPS. (PDF) This material is available free of charge via the Internet at <http://pubs.acs.org>.

AUTHOR INFORMATION

Corresponding Author

* cossairt@chem.washington.edu

Author Contributions

The manuscript was written through contributions of all authors. All authors have given approval to the final version of the manuscript.

Funding Sources

NSF CAREER Award (CHE 1552164), NSF Standard Grant (CHE-1565520 and DMR-1408617), NSF MRSEC (DMR-1420634).

ACKNOWLEDGMENT

This work was supported by the National Science Foundation under grant numbers CHE-1552164 (BMC and JLS, synthesis and characterization), CHE-1565520, and DMR-1408617 (AP and XL, theory). PDF measurement and analysis (MWT and SJLB) was supported by the NSF MRSEC program through Columbia in the Center for Precision Assembly of Superstratic and Superatomic Solids (DMR-1420634). This research used beamline 28-ID-2 of the National Synchrotron Light Source II, a U.S. Department of Energy (DOE) Office of Science User Facility operated for the DOE Office of Science by Brookhaven National Laboratory under Contract No. DE-SC0012704. Part of this work was conducted at the Molecular Analysis Facility, a National Nanotechnology Coordinated Infrastructure site at the University of Washington, which is supported in part by the National Science Foundation (grant ECC-1542101), the University of Washington, the Molecular Engineering & Sciences Institute, the Clean Energy Institute, and the National Institutes of Health. We thank the University of Washington School of Pharmacy Mass Spectrometry Center for use of their facility and helpful discussion. This work was facilitated through the use of advanced computational, storage, and networking infrastructure provided by the Hyak supercomputer system at UW, funded by the Student Technology Fee.

REFERENCES

- (1) Eilers, J.; Groeneveld, E.; de Mello Donegá, C.; Meijerink, A. Optical Properties of Mn-Doped ZnTe Magic Size Nanocrystals. *J. Phys. Chem. Lett.* **2012**, *3*, 1663–1667.
- (2) Mocatta, D.; Cohen, G.; Schattner, J.; Millo, O.; Rabani, E.; Banin, U. Heavily Doped Semiconductor Nanocrystal Quantum Dots. *Science* **2011**, *332*, 77–81.
- (3) Sytnyk, M.; Kirchschrager, R.; Bodnarchuk, M. I.; Primetzhofer, D.; Kriegner, D.; Enser, H.; Stangl, J.; Bauer, P.; Voith, M.; Hassel, A. W.; Krumeich, F.; Ludwig, F.; Meingast, A.; Kothleitner, G.; Kovalenko, M. V.; Heiss, W. Tuning the Magnetic Properties of Metal Oxide Nanocrystal Heterostructures by Cation Exchange. *Nano Lett.* **2013**, *13*, 586–593.
- (4) Yang, J.; Muckel, F.; Baek, W.; Fainblat, R.; Chang, H.; Bacher, G.; Hyeon, T. Chemical Synthesis, Doping, and Transformation of Magic-Sized Semiconductor Alloy Nanoclusters. *J. Am. Chem. Soc.* **2017**, *139*, 6761–6770.
- (5) Son, D. H.; Hughes, S. M.; Yin, Y.; Paul Alivisatos, A. Cation Exchange Reactions in Ionic Nanocrystals. *Science* **2004**, *306*, 1009–1012.
- (6) Enright, M. J.; Sarsito, H.; Cossairt, B. M. Quantifying Cation Exchange of Cd²⁺ in ZnTe: A Challenge for Accessing Type II Heterostructures. *Chem. Mater.* **2017**, *29*, 666–672.
- (7) Casavola, M.; van Huis, M. A.; Bals, S.; Lambert, K.; Hens, Z.; Vanmaekelbergh, D. Anisotropic Cation Exchange in PbSe/CdSe Core/Shell Nanocrystals of Different Geometry. *Chem. Mater.* **2012**, *24*, 294–302.
- (8) Mu, L.; Wang, F.; Sadtler, B.; Loomis, R. A.; Buhro, W. E. Influence of the Nanoscale Kirkendall Effect on the Morphology of Copper Indium Disulfide Nanoplatelets Synthesized by Ion Exchange. *ACS Nano* **2015**, *9*, 7419–7428.
- (9) Smith, A. M.; Nie, S. Bright and Compact Alloyed Quantum Dots with Broadly Tunable Near-Infrared Absorption and Fluorescence Spectra through Mercury Cation Exchange. *J. Am. Chem. Soc.* **2011**, *133*, 24–26.
- (10) Groeneveld, E.; Witteman, L.; Lefferts, M.; Ke, X.; Bals, S.; Van Tendeloo, G.; de Mello Donegá, C. Tailoring ZnSe–CdSe Colloidal Quantum Dots via Cation Exchange: From Core/Shell to Alloy Nanocrystals. *ACS Nano* **2013**, *7*, 7913–7930.
- (11) Kim, S.; Kim, T.; Kang, M.; Kwak, S. K.; Yoo, T. W.; Park, L. S.; Yang, I.; Hwang, S.; Lee, J. E.; Kim, S. K.; Kim, S.-W. Highly Luminescent InP/GaP/ZnS Nanocrystals and Their Application to White Light-Emitting Diodes. *J. Am. Chem. Soc.* **2012**, *134*, 3804–3809.
- (12) van der Stam, W.; Bladt, E.; Rabouw, F. T.; Bals, S.; de Mello Donegá, C. Near-Infrared Emitting CuInSe₂/CuInS₂ Dot Core/Rod Shell Heteronanorods by Sequential Cation Exchange. *ACS Nano* **2015**, *9*, 11430–11438.
- (13) Zhang, J.; Chernomordik, B. D.; Crisp, R. W.; Kroupa, D. M.; Luther, J. M.; Miller, E. M.; Gao, J.; Beard, M. C. Preparation of Cd/Pb Chalcogenide Heterostructured Janus Particles via Controllable Cation Exchange. *ACS Nano* **2015**, *9*, 7151–7163.
- (14) Beberwyck, B. J.; Alivisatos, A. P. Ion Exchange Synthesis of III–V Nanocrystals. *J. Am. Chem. Soc.* **2012**, *134*, 19977–19980.
- (15) De Trizio, L.; Manna, L. Forging Colloidal Nanostructures via Cation Exchange Reactions. *Chem. Rev.* **2016**, *116*, 10852–10887.
- (16) Rivest, J. B.; Jain, P. K. Cation Exchange on the Nanoscale: An Emerging Technique for New Material Synthesis, Device Fabrication, and Chemical Sensing. *Chem. Soc. Rev.* **2013**, *42*, 89–96.
- (17) Gupta, S.; Kershaw, S. V.; Rogach, A. L. 25th Anniversary Article: Ion Exchange in Colloidal Nanocrystals. *Adv. Mater.* **2013**, *25*, 6923–6944.
- (18) Beberwyck, B. J.; Surendranath, Y.; Alivisatos, A. P. Cation Exchange: A Versatile Tool for Nanomaterials Synthesis. *J. Phys. Chem. C* **2013**, *117*, 19759–19770.
- (19) Backhaus-Ricoult, M. Solid-State Reactivity at Heterophase Interfaces. *Annu. Rev. Mater. Res.* **2003**, *33*, 55–90.
- (20) Wark, S. E.; Hsia, C.-H.; Son, D. H. Effects of Ion Solvation and Volume Change of Reaction on the Equilibrium and Morphology in Cation-Exchange Reaction of Nanocrystals. *J. Am. Chem. Soc.* **2008**, *130*, 9550–9555.
- (21) Ott, F. D.; Spiegel, L. L.; Norris, D. J.; Erwin, S. C. Microscopic Theory of Cation Exchange in CdSe Nanocrystals. *Phys. Rev. Lett.* **2014**, *113*, 156803.
- (22) Zheng, Z.; Sun, Y.-Y.; Xie, W.; Zhao, J.; Zhang, S. Solvent-Based Atomistic Theory for Doping Colloidal-Synthesized Quantum Dots via Cation Exchange. *J. Phys. Chem. C* **2016**, *120*, 27085–27090.
- (23) Bothe, C.; Kornowski, A.; Tornatzky, H.; Schmidtke, C.; Lange, H.; Maultzsch, J.; Weller, H. Solid-State Chemistry on the Nanoscale: Ion Transport through Interstitial Sites or Vacancies? *Angew. Chem. Int. Ed.* **2015**, *54*, 14183–14186.
- (24) Friedfeld, M. R.; Stein, J. L.; Cossairt, B. M. Main-Group-Semiconductor Cluster Molecules as Synthetic Intermediates to Nanostructures. *Inorg. Chem.* **2017**, *56*, 8689–8697.
- (25) White, S. L.; Banerjee, P.; Chakraborty, I.; Jain, P. K. Ion Exchange Transformation of Magic-Sized Clusters. *Chem. Mater.* **2016**, *28*, 8391–8398.
- (26) White, S. L.; Smith, J. G.; Behl, M.; Jain, P. K. Co-Operativity in a Nanocrystalline Solid-State Transition. *Nat Commun* **2013**, *4*, 1–8.
- (27) van der Stam, W.; Geuchies, J. J.; Altantzis, T.; van den Bos, K. H. W.; Meeldijk, J. D.; Van Aert, S.; Bals, S.; Vanmaekelbergh, D.; de Mello Donegá, C. Highly Emissive Divalent-Ion-Doped Colloidal CsPb_{1-x}MxBr₃ Perovskite Nanocrystals through Cation Exchange. *J. Am. Chem. Soc.* **2017**, *139*, 4087–4097.
- (28) Dong, C.; van Veggel, F. C. J. M. Cation Exchange in Lanthanide Fluoride Nanoparticles. *ACS Nano* **2009**, *3*, 123–130.
- (29) De Trizio, L.; Gaspari, R.; Bertoni, G.; Kriegel, I.; Moretti, L.; Scotognella, F.; Maserati, L.; Zhang, Y.; Messina, G. C.; Prato, M.; Marras, S.; Cavalli, A.; Manna, L. Cu₃-xP Nanocrystals as a Material Platform for Near-Infrared Plasmonics and Cation Exchange Reactions. *Chem. Mater.* **2015**, *27*, 1120–1128.
- (30) Gary, D. C.; Flowers, S. E.; Kaminsky, W.; Petrone, A.; Li, X.; Cossairt, B. M. Single-Crystal and Electronic Structure of a 1.3 Nm Indium Phosphide Nanocluster. *J. Am. Chem. Soc.* **2016**, *138*, 1510–1513.
- (31) Gary, D. C.; Petrone, A.; Li, X.; Cossairt, B. M. Investigating the Role of Amine in InP Nanocrystal Synthesis: Destabilizing Cluster Intermediates by Z-Type Ligand Displacement. *Chem. Commun.* **2016**, *53*, 161–164.
- (32) Wang, R.; Ratcliffe, C. I.; Wu, X.; Voznyy, O.; Tao, Y.; Yu, K. Magic-Sized Cd₃P₂ II–V Nanoparticles Exhibiting Bandgap Photoemission. *J. Phys. Chem. C* **2009**, *113*, 17979–17982.

- (33) Adolphi, N. L.; Stoddard, R. D.; Goel, S. C.; Buhro, W. E.; Gibbons, P. C.; Conradi, M. S. The ^{31}P NMR Spectra of Cd_3P_2 and Zn_3P_2 . *J. Phys. Chem. Solids* **1992**, *53*, 1275–1278.
- (34) Anderson, N. C.; Hendricks, M. P.; Choi, J. J.; Owen, J. S. Ligand Exchange and the Stoichiometry of Metal Chalcogenide Nanocrystals: Spectroscopic Observation of Facile Metal-Carboxylate Displacement and Binding. *J. Am. Chem. Soc.* **2013**, *135*, 18536–18548.
- (35) Lawrence, K. N.; Dutta, P.; Nagaraju, M.; Teunis, M. B.; Muhoberac, B. B.; Sardar, R. Dual Role of Electron-Accepting Metal-Carboxylate Ligands: Reversible Expansion of Exciton Delocalization and Passivation of Nonradiative Trap-States in Molecule-like CdSe Nanocrystals. *J. Am. Chem. Soc.* **2016**, *138*, 12813–12825.
- (36) Xie, L.; Shen, Y.; Franke, D.; Sebastián, V.; Bawendi, M. G.; Jensen, K. F. Characterization of Indium Phosphide Quantum Dot Growth Intermediates Using MALDI-TOF Mass Spectrometry. *J. Am. Chem. Soc.* **2016**, *138*, 13469–13472.
- (37) Gary, D. C.; Terban, M. W.; Billinge, S. J. L.; Cossairt, B. M. Two-Step Nucleation and Growth of InP Quantum Dots via Magic-Sized Cluster Intermediates. *Chem. Mater.* **2015**, *27*, 1432–1441.
- (38) Beecher, A. N.; Yang, X.; Palmer, J. H.; LaGrassa, A. L.; Juhas, P.; Billinge, S. J. L.; Owen, J. S. Atomic Structures and Gram Scale Synthesis of Three Tetrahedral Quantum Dots. *J. Am. Chem. Soc.* **2014**, *136*, 10645–10653.
- (39) Stein, J. L.; Mader, E. A.; Cossairt, B. M. Luminescent InP Quantum Dots with Tunable Emission by Post-Synthetic Modification with Lewis Acids. *J. Phys. Chem. Lett.* **2016**, *7*, 1315–1320.
- (40) Frederick, M. T.; Achtyl, J. L.; Knowles, K. E.; Weiss, E. A.; Geiger, F. M. Surface-Amplified Ligand Disorder in CdSe Quantum Dots Determined by Electron and Coherent Vibrational Spectroscopies. *J. Am. Chem. Soc.* **2011**, *133*, 7476–7481.
- (41) Xie, R.; Zhang, J.; Zhao, F.; Yang, W.; Peng, X. Synthesis of Monodisperse, Highly Emissive, and Size-Tunable Cd_3P_2 Nanocrystals. *Chem. Mater.* **2010**, *22*, 3820–3822.
- (42) Glassy, B. A.; Cossairt, B. M. Ternary Synthesis of Colloidal Zn_3P_2 Quantum Dots. *Chem. Commun.* **2015**, *51*, 5283–5286.
- (43) Glassy, B. A.; Cossairt, B. M. Resolving the Chemistry of Zn_3P_2 Nanocrystal Growth. *Chem. Mater.* **2016**, *28*, 6374–6380.
- (44) Harrell, S. M.; McBride, J. R.; Rosenthal, S. J. Synthesis of Ultrasmall and Magic-Sized CdSe Nanocrystals. *Chem. Mater.* **2013**, *25*, 1199–1210.
- (45) Virieux, H.; Le Troedec, M.; Cros-Gagneux, A.; Ojo, W.-S.; Delpéch, F.; Nayral, C.; Martinez, H.; Chaudret, B. InP/ZnS Nanocrystals: Coupling NMR and XPS for Fine Surface and Interface Description. *J. Am. Chem. Soc.* **2012**, *134*, 19701–19708.
- (46) Borchert, H.; Haubold, S.; Haase, M.; Weller, H.; McGinley, C.; Riedler, M.; Möller, T. Investigation of ZnS Passivated InP Nanocrystals by XPS. *Nano Lett.* **2002**, *2*, 151–154.
- (47) Huang, K.; Demadrille, R.; Silly, M. G.; Sirotti, F.; Reiss, P.; Renault, O. Internal Structure of InP/ZnS Nanocrystals Unraveled by High-Resolution Soft X-Ray Photoelectron Spectroscopy. *ACS Nano* **2010**, *4*, 4799–4805.
- (48) Nanda, J.; Kuruvilla, B. A.; Sarma, D. D. Photoelectron Spectroscopic Study of CdS Nanocrystallites. *Phys. Rev. B* **1999**, *59*, 7473–7479.
- (49) Sowers, K. L.; Hou, Z.; Peterson, J. J.; Swartz, B.; Pal, S.; Prezhdo, O.; Krauss, T. D. Photophysical Properties of CdSe/CdS Core/Shell Quantum Dots with Tunable Surface Composition. *Chem. Phys.* **2016**, *471*, 24–31.
- (50) Subila, K. B.; Kishore Kumar, G.; Shivaprasad, S. M.; George Thomas, K. Luminescence Properties of CdSe Quantum Dots: Role of Crystal Structure and Surface Composition. *J. Phys. Chem. Lett.* **2013**, *4*, 2774–2779.
- (51) Gary, D. C.; Cossairt, B. M. Role of Acid in Precursor Conversion During InP Quantum Dot Synthesis. *Chem. Mater.* **2013**, *25*, 2463–2469.
- (52) Shen, Y.; Roberge, A.; Tan, R.; Gee, M. Y.; Gary, D. C.; Huang, Y.; Blom, D. A.; Benicewicz, B. C.; Cossairt, B. M.; Greytak, A. B. Gel Permeation Chromatography as a Multifunctional Processor for Nanocrystal Purification and on-Column Ligand Exchange Chemistry. *Chem. Sci.* **2016**, *7*, 5671–5679.
- (53) Frisch, M. J.; Trucks, G. W.; Schlegel, H. B.; Scuseria, G. E.; Robb, M. A.; Cheeseman, J. R.; Scalmani, G.; Barone, V.; Mennucci, B.; Petersson, G. A.; Nakatsuji, H. *Gaussian 09*; Wallingford, CT, USA, 2009.
- (54) Heyd, J.; Scuseria, G. E. Hybrid Functionals Based on a Screened Coulomb Potential. *J. Chem. Phys.* **2003**, *118*, 8207–8215.
- (55) Heyd, J.; Scuseria, G. E. Efficient Hybrid Density Functional Calculations in Solids: Assessment of the Heyd–Scuseria–Ernzerhof Screened Coulomb Hybrid Functional. *J. Chem. Phys.* **2004**, *121*, 1187–1192.
- (56) Vydrov, O. A.; Heyd, J.; Krukau, A. V.; Scuseria, G. E. Importance of Short-Range versus Long-Range Hartree-Fock Exchange for the Performance of Hybrid Density Functionals. *J. Chem. Phys.* **2006**, *125*, 074106.
- (57) Cho, E.; Jang, H.; Lee, J.; Jang, E. Modeling on the Size Dependent Properties of InP Quantum Dots: A Hybrid Functional Study. *Nanotechnology* **2013**, *24*, 215201.
- (58) Casida, M. E.; Jamorski, C.; Casida, K. C.; Salahub, D. R. Molecular Excitation Energies to High-Lying Bound States from Time-Dependent Density-Functional Response Theory: Characterization and Correction of the Time-Dependent Local Density Approximation Ionization Threshold. *J. Chem. Phys.* **1998**, *108*, 4439–4449.
- (59) Furche, F.; Ahlrichs, R. Adiabatic Time-Dependent Density Functional Methods for Excited State Properties. *J. Chem. Phys.* **2002**, *117*, 7433–7447.
- (60) Stratmann, R. E.; Scuseria, G. E.; Frisch, M. J. An Efficient Implementation of Time-Dependent Density-Functional Theory for the Calculation of Excitation Energies of Large Molecules. *J. Chem. Phys.* **1998**, *109*, 8218–8224.
- (61) Schaefer, H. F. *Methods of Electronic Structure Theory*, 1st ed.; Vol. 3.
- (62) Hay, P. J.; Wadt, W. R. Ab Initio Effective Core Potentials for Molecular Calculations. Potentials for the Transition Metal Atoms Sc to Hg. *J. Chem. Phys.* **1985**, *82*, 270–283.
- (63) Hay, P. J.; Wadt, W. R. Ab Initio Effective Core Potentials for Molecular Calculations. Potentials for K to Au Including the Outermost Core Orbitals. *J. Chem. Phys.* **1985**, *82*, 299–310.
- (64) Wadt, W. R.; Hay, P. J. Ab Initio Effective Core Potentials for Molecular Calculations. Potentials for Main Group Elements Na to Bi. *J. Chem. Phys.* **1985**, *82*, 284–298.
- (65) Chupas, P. J.; Xiangyun Qiu, P. J.; Hanson, J. C.; Lee, P. L.; Grey, C. P.; Billinge, S. J. L. Rapid-Acquisition Pair Distribution Function (RAPDF) Analysis. *J. Appl. Crystallogr.* **2003**, *36*, 1342–1347.
- (66) Hammersley, A. P.; Svensson, S. O.; Hanfland, M.; Fitch, A. N.; Hausermann, D. Two-Dimensional Detector Software: From Real Detector to Idealised Image or Two-Theta Scan. *High Press. Res.* **1996**, *14*, 235–248.
- (67) Juhás, P.; Farrow, C.; Yang, X.; Knox, K.; Billinge, S. Complex Modeling: A Strategy and Software Program for Combining Multiple Information Sources to Solve Ill Posed Structure and Nanostructure Inverse Problems. *Acta Crystallogr. Sect. Found. Adv.* **2015**, *71*, 562–568.
- (68) Jensen, K. M. Ø.; Juhas, P.; Tofanelli, M. A.; Heinecke, C. L.; Vaughan, G.; Ackerson, C. J.; Billinge, S. J. L. Polymorphism in Magic-Sized $\text{Au}_{144}(\text{SR})_{60}$ Clusters. *Nat. Commun.* **2016**, *7*, 11859.

TOC Graphic.

